PHYSICAL REVIEW B **86**, 140101(R) (2012)

Advanced phase-field approach to dislocation evolution

Valery I. Levitas[1] and Mahdi Javanbakht[2]
[1]*Departments of Aerospace Engineering, Mechanical Engineering, and Material Science and Engineering, Iowa State University, Ames, Iowa 50011, USA*
[2]*Department of Mechanical Engineering, Iowa State University, Ames, Iowa 50011, USA*
(Received 26 March 2012; published 9 October 2012)

The phase-field approach to dislocations is conceptually advanced. Large strain formulation is developed. A local thermodynamic potential eliminates stress dependence of the Burgers vector and reproduces the desired local stress-strain curve, as well as the desired, mesh-independent, dislocation height for any dislocation orientation. A gradient energy contains an additional term, which excludes localization of dislocation within a height smaller than the prescribed height but does not produce artificial interface energy and dislocation widening. Problems for nucleation and evolution of multiple dislocations along the single and multiple slip systems, and the interaction of dislocations with an austenite (A)-martensite (M) interface are studied using the finite element method. An unexpected scale effect in the athermal resistance to the A-M interface motion due to nucleated incoherency dislocations is revealed.

DOI: 10.1103/PhysRevB.86.140101 PACS number(s): 61.72.Ff, 61.72.Hh, 61.72.Lk, 64.70.Nd

The phase-field approach (PFA) to dislocation evolution was developed just during the past decade and is widely used for the understanding of plasticity at the nanoscale (see the pioneering papers[1–7] and reviews[8,9]). It allows one simulation of a coupled evolution of multiple interacting dislocations and a stress field without explicit tracking dislocation lines. Despite significant success, there are still a number of points for essential improvement:

(a) All of the previous studies are based on small strain (i.e., <0.1) formulation. At the same time, plastic shear γ for n dislocations is on the order of magnitude of n, which is huge for multiple dislocations. Elastic strains may also be finite, because stresses for nucleation of a dislocation are of the order of the theoretical strength. Such strains are present when the core structure should be resolved and short-range interactions of dislocations with solute atoms, other dislocations, and dislocation reactions[1,5,8] are studied. In these problems, the dislocation height H is taken as the interplanar distance d. For larger-scale simulations,[2–4] shear strain is smeared over $H \sim 100d$ of interplanar distances (and, consequently, reduced by H/d), which does not allow for representing the dislocation core correctly but does not affect stresses far from dislocations. Even for such simulations, shear strain $\gamma \sim nd/H$ is finite for $n > 0.1H/d$. Note that for large strains, spectral methods for the problem solution, developed in Refs. 1–9, are not applicable.

(b) As it was mentioned in Ref. 10, the equilibrium value of the order parameters η_i (and consequently, the Burgers vector) depends on stress tensor $\boldsymbol{\sigma}$. While in Ref. 5 this dependence was eliminated, the Burgers vector appears and grows, starting with zero stresses, similar to the case in all other theories. This causes dissipation even in the elastic region, which is contradictory in principle but may be not critical for some cases.

(c) In the models presented in Refs. 1–5 the dislocation height H is not defined by a theory but is equal to the mesh size; i.e., the theory is in principle not objective and leads to mesh-dependent solutions. When we reduced the mesh size, keeping a dislocation height H, dislocation propagates within the height of one element. The problem is not in the numerical approach but in an ill-posed problem formulation, which is similar to the problems for shear band localization.[11,12] This is because the component of the gradient of the order parameter $\nabla_n = \boldsymbol{n} \cdot \nabla\eta$, normal to the dislocation plane, does not contribute to the energy, leading to a lack of intrinsic length in this direction and a theoretically zero dislocation height.

In addition to catastrophic mesh dependence typical of ill-posed problems, it leads to high oscillating internal shear stress at the interface Σ (which should be of zero width) between the dislocation band and the rest of the crystal. This causes two opposite effects: artificial nucleation of new dislocations and generation of artificial elastic energy at the interface, which suppresses dislocation motion. Also, there is no description of how to handle dislocations inclined with respect to the mesh.

In this Rapid Communication, an advanced PFA to dislocation evolution is developed. It is objective (well posed) and based on a fully large-strain formulation. Our local thermodynamic potential is designed to eliminate the stress dependence of the Burgers vector and to reproduce the desired local stress-strain curve, as well as to obtain the desired, mesh-independent, dislocation height for any dislocation orientation. Our gradient energy contains an additional term, related to ∇_n, which excludes localization of dislocation within heights smaller than the prescribed height H but disappears at Σ; thus, it does not produce interface energy and does not lead to a dislocation widening. It is demonstrated that internal stresses at Σ can be made negligible by choosing the proper numerical approximation, otherwise, errors can be drastic. Problems for nucleation and evolution of multiple dislocations along the single and multiple slip systems, and the interaction of dislocations with an austenite (A)-martensite (M) interface are studied using the finite element method (FEM). It was found, in particular, that a sharp A-M interface loses its coherency by nucleating a dozen dislocations; the stationary spacing between them is in perfect agreement with an analytical solution. For a finite-width A-M interface, described by our PFA for phase transformations,[13,14] an unexpected scale effect is revealed. In the absence of dislocations, the A-M interface is stable only at the single critical thermal driving force X_c^0, and it is almost independent of the interface width Δ_ξ; thus, an athermal resistance to the interface motion

is absent. Generated incoherency dislocations produce an athermal threshold and hysteresis in the driving force for a direct-reverse transformation, which strongly depends on the dimensionless interface width $\bar{\Delta}_\xi = \Delta_\xi/H$. Thus, for very small and large $\bar{\Delta}_\xi$, an athermal threshold and hysteresis unexpectedly disappear.

We designate contractions of tensors $\boldsymbol{A}$ and $\boldsymbol{B}$ over one and two indices as $\boldsymbol{A}\cdot\boldsymbol{B}$ and $\boldsymbol{A}:\boldsymbol{B}$; the transpose of $\boldsymbol{A}$ is $\boldsymbol{A}^T$, $\boldsymbol{I}$ is the unit tensor, and $\otimes$ designates a dyadic product.

Model. Let $\boldsymbol{r} = \boldsymbol{r}(\boldsymbol{r}_0,t)$ be the location of a material point at time t, and $\boldsymbol{r}(\boldsymbol{r}_0,0) = \boldsymbol{r}_0$. Multiplicative decomposition of the total deformation gradient,

$$\boldsymbol{F} = \partial\boldsymbol{r}/\partial\boldsymbol{r}_0 = \boldsymbol{F}_e\cdot\boldsymbol{F}_p, \quad \boldsymbol{F}_e = \boldsymbol{V}_e\cdot\boldsymbol{R}, \tag{1}$$

into elastic and plastic parts is used; $\boldsymbol{R}$ and $\boldsymbol{V}_e$ are the lattice rotation and the elastic left stretch tensor, respectively. The plastic deformation gradient is described by an evolution equation based on the additivity of the plastic part of the velocity gradient, $\boldsymbol{l}_p := \dot{\boldsymbol{F}}_p\cdot\boldsymbol{F}_p^{-1}$, consistent with phenomenological crystal plasticity:[12]

$$\dot{\boldsymbol{F}}_p\cdot\boldsymbol{F}_p^{-1} = \sum_{\alpha=1}^{p}\sum_{\omega=1}^{m_\alpha}\frac{1}{H^\alpha}\boldsymbol{b}^{\alpha\omega}\otimes\boldsymbol{n}^\alpha\dot{\phi}(\bar{\eta}_{\alpha\omega}), \tag{2}$$

where $\phi(\bar{\eta}) = \bar{\eta}^2(3-2\bar{\eta})$, index α designates the αth slip plane with the unit normal $\boldsymbol{n}^\alpha$, and index ω is for the ωth Burgers vector $\boldsymbol{b}^{\alpha\omega}$ in each slip plane; $\eta_{\alpha\omega}$ is the order parameter for dislocations in the αth plane along the ωth slip direction, which varies between 0 and n when n dislocations appear; $\mathrm{Int}(\eta_{\alpha\omega}) = n$ and $\bar{\eta} := \eta - \mathrm{Int}(\eta_{\alpha\omega}) \in [0,1]$ are the integer and fractional parts of $\eta_{\alpha\omega}$. All parameters $(\boldsymbol{n}^\alpha,\boldsymbol{b}^{\alpha\omega},H^\alpha,\ldots)$ and the gradient operator ∇ are determined in the undeformed configuration. In contrast to PFA for phase transformations and twinning,[15] in which the finite expression $\boldsymbol{F}_p(\eta_i)$ was accepted, here we formulate the differential Eq. (2) for $\boldsymbol{F}_p$. For a single slip system, Eq. (2) can be integrated as $\boldsymbol{F}_p = \boldsymbol{I} + \frac{1}{H^\alpha}\boldsymbol{b}^{\alpha\omega}\otimes\boldsymbol{n}^\alpha[\phi(\bar{\eta}_{\alpha\omega}) + \mathrm{Int}(\eta_{\alpha\omega})]$.

The Helmholtz free energy per unit undeformed volume is accepted as $\psi = \psi(\boldsymbol{B}_e,\eta_{\alpha\omega},\nabla\eta_{\alpha\omega})$, where $\boldsymbol{B}_e = 0.5(\boldsymbol{V}_e\cdot\boldsymbol{V}_e - \boldsymbol{I})$. The thermodynamic procedure similar to that for phase transformations[13–15] and linear relationships between thermodynamic forces and fluxes results in an expression for stresses,

$$\boldsymbol{\sigma} = \frac{\rho}{\rho_0}\boldsymbol{V}_e\cdot\frac{\partial\psi}{\partial\boldsymbol{B}_e}\cdot\boldsymbol{V}_e, \tag{3}$$

and Ginzburg-Landau equations,

$$\frac{1}{L}\frac{\partial\eta_{\alpha\omega}}{\partial t} = \boldsymbol{P}^T\cdot\boldsymbol{F}_e:\frac{\partial\boldsymbol{F}_p}{\partial\eta_{\alpha\omega}} - \frac{\partial\psi}{\partial\eta_{\alpha\omega}} + \nabla\cdot\frac{\partial\psi}{\partial\nabla\eta_{\alpha\omega}}, \tag{4}$$

where L is the kinetic coefficient, and $\boldsymbol{\sigma}$ and $\boldsymbol{P}$ are the true Cauchy stress tensor and the nonsymmetric Piola-Kirchhoff stress tensor (force per unit area in the undeformed configuration). We accept the expression for

$$\psi = \psi^e(\boldsymbol{B}_e) + \sum_{\alpha=1}^{p}\sum_{\omega=1}^{m_\alpha}A_\alpha\bar{\eta}_{\alpha\omega}^2(1-\bar{\eta}_{\alpha\omega})^2 + \frac{\beta}{2}\sum_{\alpha=1}^{p}\sum_{\omega=1}^{m_\alpha}\{(\nabla\bar{\eta}_{\alpha\omega})^2 + [M(1-\bar{\eta}_{\alpha\omega})^2 - 1](\nabla\bar{\eta}_{\alpha\omega}\cdot\boldsymbol{n}_\alpha)^2\} \tag{5}$$

as the sum of elastic, crystalline, and gradient energy. The coefficient A_α is a periodic stepwise function of the coordinate along the normal to the slip plane $\boldsymbol{n}_\alpha$, which is equal to $A_{0\alpha}$ within the dislocation band of the height H_α and $kA_{0\alpha}$ ($k \gg 1$) in a thin boundary layer between dislocations of the width $w_\alpha = pH_\alpha$ ($p \ll 1$). This function determines the dislocation height independent of the computational mesh, which makes our equations objective. The $\eta_{\alpha\omega}$ dependence of $\boldsymbol{F}_p$ and the crystalline energy is obtained from conditions that for homogeneous states, the stationary solutions of Eq. (4) are $\eta_{\alpha\omega} = n$ for any stresses, which provides independence of the Burgers vector of the stress. Another solution results in the equilibrium resolved shear stress $\tau-\bar{\eta}$ relationship

$$\tau_{\alpha\omega} = \boldsymbol{n}_\alpha\cdot\boldsymbol{F}_p\cdot\boldsymbol{P}^T\cdot\boldsymbol{F}_e\cdot\frac{\boldsymbol{b}^{\alpha\omega}}{|\boldsymbol{b}^{\alpha\omega}|} = \tau_{\alpha\omega}^c(1-2\bar{\eta}_{\alpha\omega}), \tag{6}$$

where $\tau_{\alpha\omega}^c = A_{\alpha\omega}/3\gamma_{\alpha\omega}$ is the critical shear stress; $\gamma_{\alpha\omega} = |\boldsymbol{b}^{\alpha\omega}|/H_\alpha$ is the plastic shear strain. Equation (6), in contrast to previous models, has the following desired features: Dislocation does not nucleate (i.e., $\bar{\eta}_{\alpha\omega} = 0$) for $-\tau_{\alpha\omega}^c < \tau_{\alpha\omega} < \tau_{\alpha\omega}^c$, i.e., there is no artificial dissipation in the elastic region; after nucleation (i.e., $\bar{\eta}_{\alpha\omega} \neq 0$), stress reduces monotonously with increasing $\bar{\eta}_{\alpha\omega}$, i.e., material instability will lead to $\bar{\eta}_{\alpha\omega} \to 1$.

If $M = 0$, the gradient energy in Eq. (5) coincides with known expressions.[2–5] However, for $M = 0$, after nucleation, dislocation propagates within a band of one finite element high, which is unphysical. An additional term with $M \ll 1$ penalizes gradients along the normal $\boldsymbol{n}_\alpha$, which leads to dislocation propagation within the entire band of the height H. It is localized at the propagation front, disappears when dislocation is completed ($\bar{\eta}_{\alpha\omega} = 1$), and does not produce artificial surface energy at the boundary Σ.

The equilibrium equation $\nabla\cdot\boldsymbol{P} = \boldsymbol{0}$ is included. The isotropic quadratic elastic potential ψ^e in terms of finite elastic strain $\boldsymbol{V}_e-\boldsymbol{I}$ (Ref. 16) was used for simplicity in all examples. To resolve a dislocation core and interaction between the phase interface and dislocations, we use $H^\alpha = 2d^\alpha$ in all problems. However, for larger-scale simulations, one can use $H^\alpha = 100d^\alpha$ as in Refs. 2–4. The following parameters for all slip systems have been used in all problems, unless stated differently: $\beta = 8.76\times10^{-11}$ N, $A_0 = 1.43\times10^9$ N/m, $L = 10^4$ (Pa s)$^{-1}$, $M = 0.1$, $\gamma = 0.5$, $k = 100$, $H = 0.7$ nm, $w = 0.1H$, $|\boldsymbol{b}| = 0.35$ nm, shear modulus $\mu = 71.5$ GPa, and bulk modulus $K = 112.6$ GPa.

In our simplified PFA to interaction of dislocations and phase transformations, we use $\boldsymbol{F} = \boldsymbol{F}_e\cdot\boldsymbol{F}_t\cdot\boldsymbol{F}_p$ and all equations and properties for phase transformations from Ref. 14, including the equation for the transformation deformation gradient $\boldsymbol{F}_t$. It is not our goal here to develop a general theory for the interaction of dislocations and phase transformations. However, to make the first step toward such a theory and to illustrate our PFA to dislocations with the nontrivial and challenging problems, we included problems that do not require a general theory for such an interaction. Namely, we consider dislocations either solely in austenite (assuming, e.g., a much higher yield strength of martensite) or at the austenite-martensite interface.

Numerical solutions. The FEM approach and the code COMSOL with the embedded remeshing procedure were used. Plane strain problems for straight edge dislocations are considered. All size, stress, and time parameters are normalized by the dislocation height H, τ_c, and characteristic time

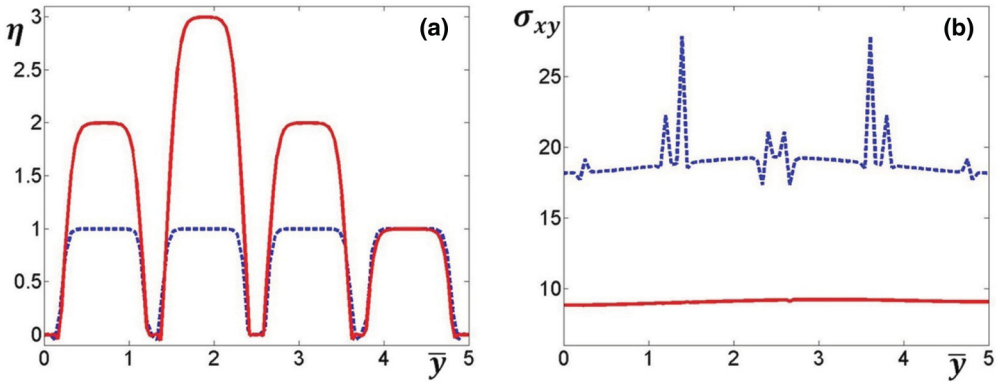

FIG. 1. (Color online) Distribution of the order parameter (a) and shear stress σ_{xy} (b) at $\bar{t} = 10$ in a rectangular sample for the fifth degree polynomial in space coordinates for both η and displacements (solid red line, mesh-independent solution), and for the second degree polynomial for η and fifth degree polynomial for displacements (blue dashed line).

$1/(AL)$, respectively. The η profile for a single dislocation coincided with an analytical expression from Ref. 17.

(1) A comprehensive parametric study of the accuracy of the numerical solution was performed. As an example, a rectangle with a size of 5×21.5 is considered, with the upper side fixed in the y direction and the lower side in both x and y directions; lateral sides are stress free. Macroscopic simple shear strain is applied: The horizontal displacement $\bar{u} = 0.4\bar{t}$ is applied at the upper side from $\bar{t} = 0$ to 5, and then $\bar{u} = 2$ from $\bar{t} = 5$ to 10. Multiple potential horizontal dislocation bands are introduced by prescribing a corresponding periodic function for the threshold A^{α}. The initial condition is $\eta = 0.01$ in a small region at the left side of the bands and zero everywhere else. The material properties are listed above except $A_0 = 0.36 \times 10^9$ N/m and $\gamma = 0.25$. Unstructured FEM mesh was used. In Fig. 1, distribution of the order parameter and shear stress σ_{xy} at $\bar{t} = 10$ is presented for the fifth degree interpolation polynomial in the FEM in space coordinates for both η and displacements (solid red line, mesh-independent solution), and for the second degree interpolation polynomial for η and fifth degree polynomial for displacements (blue dashed line). Results differ drastically. One of the main natural requirements to the solution is that after passing of dislocations through any chosen region, boundaries of the dislocation bands Σ do not generate internal stresses. For the lower degree polynomial, significant unphysical internal shear stresses (oscillations) at the boundaries Σ are present even after the appearance of the first dislocation. These oscillations produce artificial interface energy, which suppresses propagation of dislocations; that is why solutions for different FEM approximations are very different, including a different number of dislocations and, consequently, the degree of relaxation of elastic stresses. They cause artificial nucleation of dislocations for other situations. At the same time, for a fifth degree polynomial for both fields, internal stresses and oscillations are negligible even after the appearance of multiple dislocations. The obtained results illustrate the potential danger of obtaining physically wrong solutions unless their correctness is proven.

(2) A rectangle with a size of 7.14×57.14 was considered with a sharp A-M interface in the middle of it and in the middle of a dislocation band (Fig. 2). A misfit (transformation) strain of $\delta = 0.1$ in the x direction is applied in the upper martensitic half of the sample. The upper and lower sides are fixed in the y direction; all other external stresses are zero. The initial condition was $\eta = 0.01$ inside the dislocation band. The interface loses its coherence by nucleating dislocations at the free surface, one by another, which propagate along the interface.[18] In the stationary state, the distance between any of two neighboring dislocations is 5, in perfect correspondence with the analytical expression $|\boldsymbol{b}|/(\delta H)$. Eleven dislocations produce a step at the free surface with a shear strain of $n\gamma = 5.5$, which clearly requires large-strain formulation.

(3) *Parallel dislocation system*. A rectangle of a size of 7.4×14.26 was considered with the upper and lower sides fixed in the y direction and the left bottom corner fixed in both directions. This problem models dislocation activity near the lath martensite unit, which is located at the left side of the sample and possesses a transformation shear strain of 0.3 (Fig. 3 and Ref. 18). Initially, there are no dislocations ($\eta = 0$), except in a small region along the inclined A-M interface with $\eta = 0.01$. Elastic stresses lead to nucleation and propagation of parallel dislocations, one after another, with two or three in each system in the stationary state. Relaxation of elastic stresses leads to straightening of the initially curved interface. Dislocations do not move outside the prescribed bands, have clear horizontal boundaries (despite the unstructured FEM mesh), and propagate acceptably quasihomogeneously [similar to problem (1) discussed above]. Moreover, the solution is mesh independent for more than six elements per band.

(4) *Interaction of the evolving A-M interface and dislocations*. Both phase transformation and dislocation evolution

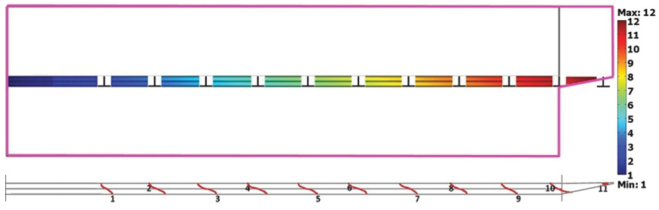

FIG. 2. (Color online) Stationary distribution of dislocations that appeared at the free surface and propagated along the sharp A-M interface with a misfit strain of 0.1 in the x direction. The right symmetric half of a sample is shown.

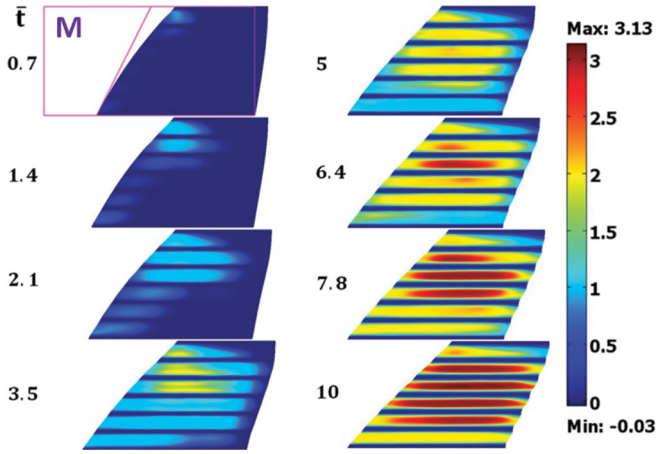

FIG. 3. (Color online) Evolution of a parallel dislocation system in austenite under prescribed transformation shear strain in the martensitic part of a sample.

are described by a PFA. A sample and boundary conditions are the same as for problem (2). First, the stationary solution for the horizontal finite-width A-M interface, described by the order parameter ξ and located at the center of a sample, was obtained without dislocations, which was taken as an initial condition for a coupled problem with dislocations. A transformation strain of $\delta = 0.1$ in the x direction is applied in the upper martensitic half of the sample, as for problem (2). A dislocation band is located at the middle of the sample (Fig. 4). The initial condition is $\eta = 0.01$ inside the dislocation band. Various interface widths $\bar{\Delta}$ have been obtained by varying the magnitude of the potential barrier A_0 for martensitic transformation [similar to A_α in Eq. (5)].

Coupled evolution of the phase transformation (PT) and dislocations for the interface width $\bar{\Delta}_\xi = 7.37$ and the thermal driving force $X = (1 - \theta/\theta_e)/(1 - \theta_c/\theta_e) = 0.008$ for a martensitic PT for an initially coherent A-M interface is shown in Fig. 4 and Ref. 18; here θ, θ_e, and θ_c are the temperature, the phase equilibrium temperature for A-M, and the critical temperature for the loss of A stability. While dislocations nucleate from the free surface and propagate, at the central part of the sample the interface broadens and finally material

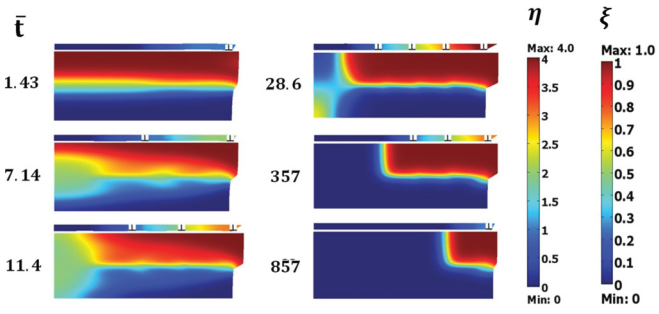

FIG. 4. (Color online) Coupled evolution of the phase transformation order parameter ξ and corresponding dislocation order parameter η for the interface width $\bar{\Delta}^*_\xi = 7.37$ and the driving force $X = 0.008$ for an initially coherent A-M interface in half of a sample. The thin band above the sample shows the evolution of edge dislocations along the A-M interface. Finally, both martensite and misfit dislocations disappear.

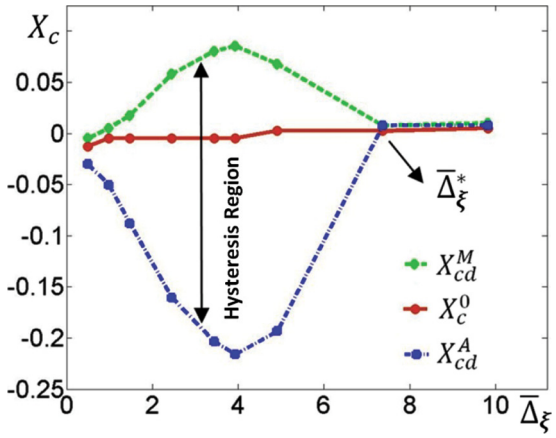

FIG. 5. (Color online) Critical thermodynamic driving force X_c to cause complete transformation in a sample vs a relative interface width $\bar{\Delta}_\xi$ for the problem in Fig. 4. The middle line is for a coherent interface, which does not exhibit any hysteresis. The upper and lower lines are for the transformation to M and A, respectively, coupled to a dislocation evolution. In the region between these lines the interface does not evolve, i.e., dislocations produce a scale-dependent hysteresis region.

transforms to A. Dislocations stabilize the horizontal interface, however, the vertical interface propagates into the M region, pushing dislocations back. Finally, both martensite and misfit dislocations disappear.

The dependence of the critical driving force X_c to cause a complete transformation in a sample versus $\bar{\Delta}_\xi$ is presented in Fig. 5. We considered an A-M interface width range of $0.49 < \bar{\Delta}_\xi < 9.83$. In the absence of dislocations, the coherent A-M interface is stable only at the specific thermodynamic driving force X_c and it is almost independent of $\bar{\Delta}_\xi$. A small nonzero $X^0_c \simeq \pm 0.005$ is caused by internal stresses and geometric changes due to transformation strain. In the presence of dislocations and for a range of $\bar{\Delta}_\xi$, the A-M interface is stabilized within a range of X ($X^{\mathrm{A}}_c < X < X^{\mathrm{M}}_c$); at $X > X^{\mathrm{M}}_c$, the material transforms to M and at $X < X^{\mathrm{A}}_c$ it transforms to A. Thus, incoherency dislocations produce athermal resistance to the interface motion, which is expected. What is surprising is that this athermal threshold is strongly size dependent, with a maximum at $\bar{\Delta}_\xi = 4.91$ for transformations in both directions. Hysteresis disappears at the critical $\bar{\Delta}^*_\xi = 7.37$, which is completely unexpected. Also, for small $\bar{\Delta}_\xi$, hysteresis reduces to a small value. The asymmetry of the curves in Fig. 5 with respect to zero is caused by an asymmetry of the deformed geometry.

To summarize, an advanced PFA to dislocations is developed and a number of problems on dislocation evolution and the interaction between phase transformations and dislocations are solved. A strong scale dependence of the athermal threshold for the interface propagation due to the generation of dislocation is revealed. A similar approach can be developed for partial dislocations and extended for dislocation reactions, and detailed interactions between phase transformations and plasticity.

The support of NSF, ARO, DTRA, and ISU is gratefully acknowledged.

[1]C. Shen and Y. Wang, Acta Mater. **52**, 683 (2004).
[2]Y. U. Wang, Y. M. Jin, A. M. Cuitino, and A. G. Khachaturyan, Acta. Mater. **49**, 1847 (2001).
[3]Y. M. Jin and A. G. Khachaturyan, Philos. Mag. Lett. **81**, 607 (2001).
[4]Y. U. Wang, Y. M. Jin, and A. G. Khachaturyan, Acta. Mater. **51**, 4209 (2003).
[5]S. Y. Hu, Y. L. Li, Y. X. Zheng, and L. Q. Chen, Int. J. Plast. **20**, 403 (2004).
[6]M. Koslowski, A. M. Cuitino, and M. Ortiz, J. Mech. Phys. Solids **50**, 2597 (2002).
[7]M. Koslowski and M. Ortiz, Modell. Simul. Mater. Sci. Eng. **12**, 1087 (2004).
[8]Y. U. Wang and J. Li, Acta. Mater. **58**, 1212 (2010).
[9]J. Kundin, H. Emmerich, and J. Zimmer, Philos. Mag. **91**, 97 (2011).
[10]V. I. Levitas, D. L. Preston, and D.-W. Lee, Phys. Rev. B **68**, 134201 (2003).
[11]H. M. Zbib and E. C. Aifantis, Acta Mech. **92**, 209 (1992); R. K. Abu Al-Rub and G. Z. Voyiadjis, Int. J. Numer. Methods Eng. **63**, 603 (2005).
[12]V. A. Lubarda, *Elastoplasticity Theory* (CRC, Boca Raton, FL, 2002).
[13]V. I. Levitas and M. Javanbakht, Phys. Rev. Lett. **105**, 165701 (2010).
[14]V. I. Levitas and M. Javanbakht, Phys. Rev. Lett. **107**, 175701 (2011).
[15]V. I. Levitas, V. A. Levin, K. M. Zingerman, and E. I. Freiman, Phys. Rev. Lett. **103**, 025702 (2009).
[16]A. I. Lurie, *Nonlinear Theory of Elasticity* (North-Holland, Amsterdam, 1990).
[17]D.-W. Lee, H. Kim, A. Strachan, and M. Koslowski, Phys. Rev. B **83**, 104101 (2011).
[18]See Supplemental Material at http://link.aps.org/supplemental/10.1103/PhysRevB.86.140101 for movies.